Nanoscale

PAPER

View Article Online
View Journal | View Issue

Cite this: *Nanoscale*, 2015, **7**, 9731

Continuous crafting of uniform colloidal nanocrystals using an inert-gas-driven microflow reactor†

Hailong Tang,[a,b] Yanjie He,[a] Bo Li,[a] Jaehan Jung,[a] Chuchu Zhang,[a] Xiaobo Liu*[b] and Zhiqun Lin*[a]

Recent research has witnessed rapid advances in synthesis of nanocrystals, which has led to the development of a large variety of approaches for producing nanocrystals with controlled dimensions. However, most of these techniques lack the high-throughput production. Herein, we report on a viable and robust strategy based on an inert-gas-driven microflow reactor for continuous crafting of high-quality colloidal nanocrystals. With the judicious introduction of the inert-gas driven capability, the microflow reactor provides an attractive platform for continuous production of colloidal nanocrystals in large quantities, including easily-oxidized nanocrystals. The as-synthesized nanocrystals possessed a uniform size and shape. Intriguingly, the size of nanocrystals can be effectively tailored by varying the flow rate and the precursor concentration. We envision that the microflow reactor strategy is general and offers easy access to a wide range of scalable nanocrystals for potential applications in sensors, optics, optoelectronics, solar energy conversion, batteries, photocatalysis, and electronic devices.

Received 7th March 2015,
Accepted 23rd April 2015

DOI: 10.1039/c5nr01492a

www.rsc.org/nanoscale

1. Introduction

Advances in the colloidal synthesis of high-quality nanocrystals of myriad dimensions, compositions, and architecture have opened up new opportunities to explore their unique size and shape dependent properties (*e.g.*, optical, electronic, and magnetic) and exploit them as functional constituents and promising building blocks for use in solar cells,[1–3] catalysis,[4,5] hydrogen generation,[6,7] thermoelectrics,[8,9] bioimaging,[10,11] biosensors,[12] *etc*. Despite their promising applications noted above, it remains a great challenge to achieve scalable production for more commercially viable applications.[13] Obviously, the simplest means of increasing the production volume is to scale up the reaction vessel. However, as the vessel size becomes larger, it would be extremely difficult to control the reaction temperature and accomplish homogeneous mixing, thereby leading to nanocrystals with non-uniformity and poor size control, thus affecting their physical and chemical properties.[14] In this context, it is highly desirable to expand the possibilities for development of scalable and low-cost techniques to increase the productivity of nanocrystals.

In recent years, a flow reactor based on the use of reactors in the form of a continuous flow of reaction solution has emerged as an alternative route to scale-up the production of nanomaterials.[15] In sharp contrast to conventional large batch production, a flow reactor has several attractive features, including fast heat transfer due to the high surface area to volume ratio, fast mass transfer in a relatively small volume,[16] and no limitation in producing large quantities of nanomaterials in continuous flow. We noted that some protocols originally developed using batch reactors have been modified and successfully extended to continuous flow reactors. In spite of the several types of nanocrystals[17–21] that have been prepared using continuous flow reactors, the ability to synthesize colloidal nanocrystals, which have a strong tendency to be oxidized by employing continuous flow reactors, has yet to be explored. All current state-of-art flow reactors are driven by a syringe or pump, which cannot prevent these readily oxidized nanocrystals from oxidation at high temperatures during the synthesis.

[a]*School of Materials Science and Engineering, Georgia Institute of Technology, Atlanta, GA 30332, USA. E-mail: zhiqun.lin@mse.gatech.edu*
[b]*High Temperature Resistant Polymers and Composites Key Laboratory of Sichuan Province, School of Microelectronics and Solid-State Electronics, University of Electronic Science and Technology of China, Chengdu 610054, China. E-mail: liuxb@uestc.edu.cn*

†Electronic supplementary information (ESI) available: The schematic illustration of five functional sections and a digital image of the inert-gas-driven continuous microflow reactor are shown in Fig. S1. The digital images and PL spectrum of the Cu_2S nanocrystals are shown in Fig. S2 and S3, respectively. TEM images of 2-D and 3-D self-assemblies of Cu_2S nanocrystals are shown in Fig. S4. The experimental procedures for synthesis of Ag nanocrystals are provided, together with a TEM image, size distribution histogram and UV-vis spectrum (Fig. S5). See DOI: 10.1039/c5nr01492a

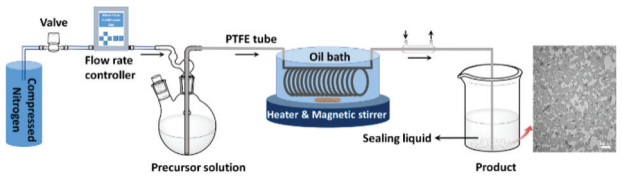

Fig. 1 Schematic illustration of an inert-gas-driven microflow reactor for continuous synthesis of nanocrystals. The last panel shows a representative TEM image of as-synthesized Cu_2S nanocrystals, and the scale bar is 100 nm.

Herein, we developed a novel inert-gas-driven continuous microflow reactor (Fig. 1 and Fig. S1†) to attain continuous production of colloidal nanocrystals, in particular easily-oxidized p-type semiconductor Cu_2S nanocrystals. Monodisperse Cu_2S nanocrystals with a well-controlled size and nearly monodisperse size distribution were, for the first time, crafted in large quantities capitalizing on the microflow reactor. Quite intriguingly, the size of nanocrystals can be readily tuned by independently varying the flow rate and the precursor concentration. In addition to Cu_2S nanocrystals, semiconducting Cu_2O and plasmonic Ag nanocrystals were also synthesized using a continuous microflow reactor. The resulting nanocrystals possessed uniform size and shape. Clearly, the judicious introduction of the inert-gas-driven capability into the microflow reactor renders the mass-production of a large variety of other easily-oxidized nanocrystals for promising applications in optical, electronic, optoelectronic, sensory, catalytic, and magnetic materials and devices.

2. Experimental section

2.1. Design and assembly of inert-gas-driven continuous microflow reactor

The experimental setup of the inert-gas-driven continuous microflow reactor for nanocrystal synthesis is shown in Fig. 1 and Fig. S1.† The microflow reaction system was composed of five functional sections as follows: (1) inert-gas-driven; (2) flow rate controller; (3) pressure controlled feed; (4) flow reactor; and (5) product collection. As a key section, a polytetrafluoroethylene (PTFE) tube (inner diameter = 1.588 mm) was used as a flow reactor due to the high thermal stability and excellent chemical inertia of PTFE. The length of the PTFE tube immersed in the oil bath was fixed at 15.2 m (equivalent volume = 30 mL). A mass flow controller (MicroTrak™ Model 101, Sierra Instruments) was utilized to control the flow rate of inert gas (*i.e.*, nitrogen) within the range of 0.10–4.00 mL min^{-1}. Thus, the reaction time can be precisely varied from 7.5 min (30 mL divided by 4.00 mL min^{-1}) to 5 h (30 mL divided by 0.10 mL min^{-1}) by tuning the flow rate. It is worth noting that the PTFE tube with any desired length can be readily employed to adjust the limitation of the reaction time. Furthermore, as the reaction temperature also plays a crucial role in the quality of as-synthesized nanocrystals, a magnetic stirrer was applied in the oil bath for reaching a homogeneous temperature. To avoid the oxidization of easily oxidized nanocrystals, the reaction solution was cooled to ambient temperature prior to the collection of the final product, which was collected in a sealing liquid (*e.g.*, ethanol, methanol, *etc.*).

2.2. Synthesis of colloidal nanocrystals

In a typical synthesis of colloidal nanocrystals, high purity nitrogen was introduced into the microflow reactor and subsequently into the sealing liquid for 1 h to completely remove oxygen in the reactor. The oil bath was preheated to the desired temperature (*e.g.*, 190 °C for Cu_2S nanocrystals, and 150 °C for Cu_2O and Ag nanocrystals). Afterwards, the premade precursor solution was injected into the reaction vessel (*i.e.*, a two-necked flask in section (3) in Fig. S1†), and forced to enter the PTFE tubular reactor by pressurizing nitrogen at a controlled flow rate. Subsequently, the reaction product was cooled to ambient temperature by flushing the PTFE tube with cold water, and collected in the sealing liquid. Finally, the product was purified by centrifuging at 6500 rpm for 10 min and washing with organic solvents (*i.e.*, chloroform for Cu_2S nanocrystals, ethanol for Cu_2O nanocrystals, and methanol for Ag nanocrystals). The purification process was repeated three times.

2.3. Characterization

The morphology of colloidal nanocrystals was imaged by using a transmission electron microscope (TEM, JEOL JEM 100CX) working at 100 kV and a high-resolution transmission electron microscope (HRTEM, FEI Tecnai F30) working at 300 kV. TEM samples were prepared by drop-casting nanocrystals dispersed in chloroform or ethanol onto carbon-coated copper TEM grids (400 mesh, Electron Microscopy Sciences). The energy dispersive X-ray (EDX) analyses were performed on a LEO 1550 Field Emission Scanning Electron Microscope equipped with an Oxford Energy Dispersive Spectrometer. For EDX characterization, the nanocrystals were drop-cast on a silicon substrate. Powder X-ray diffraction (XRD) was performed at room temperature on an X'pert PRO Alpha-1 diffractometer with Cu Kα radiation (λ = 1.54 Å). A Renishaw InVia Raman microscope was used for recording both the Raman scattering and photoluminescence (PL) emission spectra of Cu_2S nanocrystals. A 532 nm laser with the power set at 500 mW was utilized as the excitation light source of the Raman scattering spectrum. A 785 nm laser with the power set at 50 mW was applied as the excitation light source for the PL emission measurement. The ultraviolet-visible-near infrared (UV-vis-NIR) absorption spectra were recorded using a Shimadzu 2600 UV-vis spectrophotometer.

3. Results and discussion

We first crafted Cu_2S nanocrystals to demonstrate the effectiveness of our inert-gas-driven microflow reactor strategy in producing large-quantity easily-oxidized nanocrystals (see the

Experimental section). The choice of Cu_2S as the model nanocrystals to be synthesized was motivated by the fact that it is a p-type semiconductor with a relatively low bandgap of 1.2 eV for potential applications in solar cells,[22,23] cold cathodes,[24] nanoscale switches,[25] among other areas. In a typical reaction, 1.0 mmol of copper(II) acetylacetonate [$Cu(acac)_2$, 99.99%, Aldrich] was dissolved in a mixture of 1-dodecanethiol (DDT, 98%, Aldrich; 10–40 mL) and 1-octadecene (ODE, 90%, Alfa; 40 mL) to yield the precursor solution, in which DDT served as the sulfur source, ligand, and reducing agent. In order to prevent clogging of the tubular reactor by inorganic colloids, the concentration of precursor solution (*i.e.*, 12.5–20 mmol L^{-1}) was greatly reduced in comparison with the batch synthesis (typically 100 mmol L^{-1}).[26] Accordingly, it reduced the nanocrystal production rates. The precursor solution was vacuumed for 5 min to remove oxygen under vigorous magnetic stirring. The precursor solution was then introduced into the microflow reactor system which had been purged with nitrogen for 1 h. The flow rate of the precursor solution in the PTFE tube was controlled at 0.25 mL min^{-1}, which is equivalent to the reaction time of 2 h (*i.e.*, 30 mL/0.25 mL min^{-1} = 2 h). The nanocrystal production rates (milligram per hour; mg h^{-1}) were approximately 24 mg h^{-1}, 20 mg h^{-1} and 15 mg h^{-1} at the DDT/ODE ratios of 10/40, 20/40 and 40/40, respectively. This relatively low production rate was primarily due to the low concentration of precursor solution and the long reaction time. Nevertheless, a multifold increase in throughput may be easily achieved through the use of multiple identical reaction channels.[15] DDT-capped Cu_2S nanocrystals were obtained after purification by centrifuging and rinsing with chloroform (see the Experimental section). The final Cu_2S nanocrystals were highly soluble in various organic solvents (*e.g.*, chloroform, toluene, hexane) due to the surface passivation by the DDT ligand (Fig. S2†).

Interestingly, different sized Cu_2S nanocrystals can be prepared by tuning the volume ratio of DDT to ODE (*i.e.*, the DDT concentration). The TEM images and the corresponding size distribution histograms of Cu_2S nanocrystals synthesized at different DDT/ODE ratios are shown in Fig. 2. The average diameters of Cu_2S nanocrystals synthesized at the DDT/ODE ratios of 10/40, 20/40, and 40/40 are 8.8 ± 0.9 nm, 11.2 ± 0.8 nm, and 13.5 ± 0.9 nm, respectively, as determined by the statistical analysis. Clearly, the diameter of Cu_2S nanocrystals increased with the increasing DDT/ODE ratio. It has been reported that the metal thiolate intermediate compound was formed first, and this compound was then decomposed into metal sulfide nanocrystals with a prolonged reaction time.[26,27] Therefore, a larger DDT/ODE ratio (*i.e.*, higher DDT concentration) led to a higher copper thiolate concentration, which resulted in the formation of larger sized nanocrystals due to the repetitive nucleation process. On the other hand, the size of Cu_2S nanocrystals decreased from 13.5 ± 0.9 nm to 9.6 ± 1.0 nm as the flow rate increased from 0.25 mL min^{-1} (corresponding to a 2 h reaction time) to 0.33 mL min^{-1} (*i.e.*, a 1.5 h reaction time) when the volume ratio of DDT/ODE was kept at 40 : 40 (Fig. 2e, f and 3). Taken together, it is clear that by manipulating the volume ratio of DDT to ODE and regulating the flow rate, the size of Cu_2S nanocrystals can be effectively controlled, as summarized in Table 1.

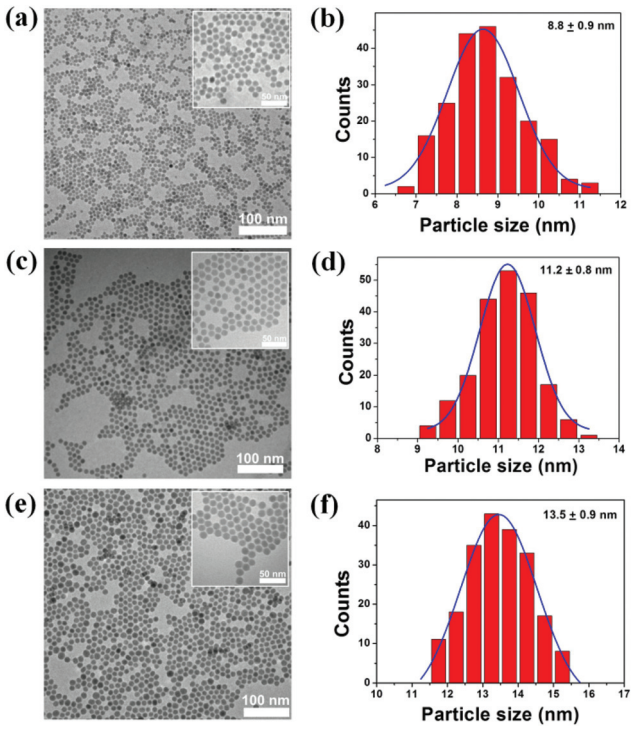

Fig. 2 TEM images and the corresponding size distribution histograms of Cu_2S nanocrystals synthesized at 190 °C at a flow rate of 0.25 ml min^{-1} (*i.e.*, a reaction time of 2 h) with different volume ratios of DDT : ODE: (a, b) 10 : 40, (c, d) 20 : 40, and (e, f) 40 : 40. The close-ups of TEM images are shown as insets in (a), (c) and (e), respectively. The blue curves were the Gaussian fittings of nanocrystal size distributions.

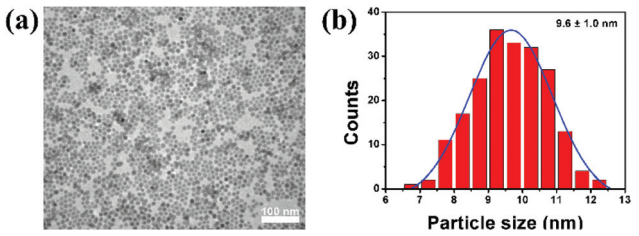

Fig. 3 (a) TEM image, and (b) the corresponding size distribution histogram of Cu_2S nanocrystals synthesized at 190 °C at a flow rate of 0.33 mL min^{-1} (*i.e.*, corresponding to a reaction time of 1.5 h) with a volume ratio of DDT : ODE at 40 : 40.

Furthermore, the flow pattern played a crucial role in the size distribution of Cu_2S nanocrystals. For flow in a tube, the Reynolds number (Re) of fluid can be calculated according to the following equation:[28]

$$\mathrm{Re} = \frac{\rho V D}{\mu} \quad (1)$$

Table 1 Effect of the DDT/ODE ratio and flow rate on the diameter of Cu_2S nanocrystals

Cu_2S sample	DDT : ODE (v/v)	Flow rate (mL min^{-1})	Reaction time (h)	Reynolds number	Diameter (nm)
Fig. 2a	10 : 40	0.25	2	0.9	8.8 ± 0.9
Fig. 2c	20 : 40	0.25	2	0.9	11.2 ± 0.8
Fig. 2e	40 : 40	0.25	2	0.9	13.5 ± 0.9
Fig. 3a	40 : 40	0.33	1.5	1.2	9.6 ± 0.9

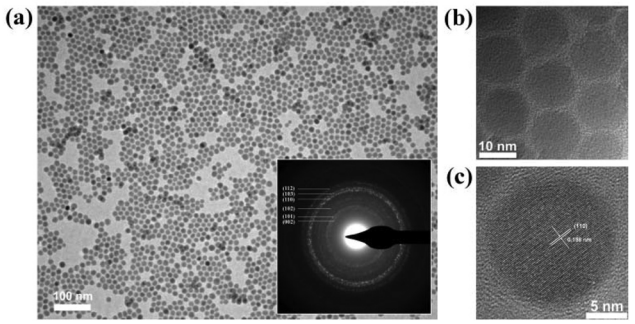

Fig. 4 (a) A representative TEM image of 13.5 ± 0.9 nm Cu_2S nanocrystals. The SAED patterns are shown as the inset. (b, c) HRTEM images of 13.5 nm Cu_2S nanocrystals, in which the crystalline lattice is clearly evident.

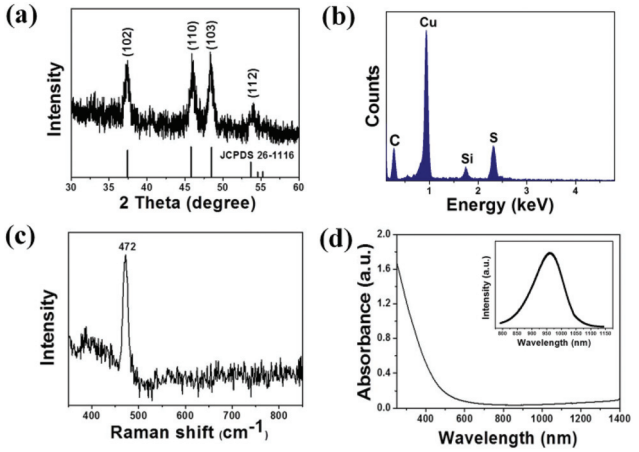

Fig. 5 (a) XRD pattern of Cu_2S nanocrystals. The standard diffraction of Cu_2S (JCPDS no. 26-1116) is also shown at the bottom as a reference. (b) EDS and (c) Raman spectra of Cu_2S nanocrystals. In the EDS spectrum, the Si signal is from the silicon wafer used. (d) UV-vis-NIR absorption spectrum of Cu_2S nanocrystals. The inset shows the NIR photoluminescence emission spectrum of Cu_2S nanocrystals at room temperature under the 785 nm excitation.

where ρ and μ are the density and dynamic viscosity of fluid, respectively. V is the linear flow velocity, and D is the inner diameter of the PTFE tube. In this study, we assumed that the solutes did not drastically change the viscosity of the fluid and thus the viscosity of the solvent was used.[21] Based on the calculation, the Reynolds numbers Re for the synthesis of Cu_2S nanocrystals were approximately 0.9 and 1.2 at the flow rates of 0.25 mL min^{-1} and 0.33 mL min^{-1} respectively (Table 1), which were smaller than the critical value of 2100 by several orders of magnitude. Clearly, the flows were laminar, leading to the formation of Cu_2S nanocrystals with nearly monodisperse size distribution.

The representative TEM and HRTEM images of Cu_2S nanocrystals with an average diameter of 13.5 ± 0.9 nm are shown in Fig. 4a and b, respectively. Obviously, Cu_2S nanocrystals possessed uniform size and shape, and were nearly monodisperse. The HRTEM image revealed that Cu_2S nanocrystals had good crystallinity (Fig. 4c). The corresponding lattice fringes with an interplanar distance of 0.198 nm can be indexed to the (110) planes of hexagonal Cu_2S, indicating that the nanocrystals were terminated by the {001} planes.[29] Furthermore, the selected area electron diffraction (SAED) patterns (the inset in Fig. 4a) showed several distinct rings and the calculated d-spacings correlated well with interplanar distances of hexagonal Cu_2S. The X-ray diffraction (XRD) measurement was performed to further confirm the crystallographic structure of Cu_2S nanocrystals. The XRD pattern of the 13.5 nm Cu_2S nanocrystals displayed four peaks at 2θ = 37.4°, 45.8°, 48.5°, and 53.7° corresponding to (102), (110), (103), and (112) lattice planes, which are in good agreement with the standard spectrum of hexagonal Cu_2S (JCPDS no. 26-1116 in Fig. 5a). The EDX analysis verified the presence of Cu and S elements in nanocrystals with an appropriate stoichiometry of Cu_2S (Fig. 5b). The signal of the C element was derived from 1-dodecanethiol, which was capped on the surface of nanocrystals as the stabilizing ligand. Furthermore, the Raman spectrum of nanocrystals clearly showed a characteristic peak at 472 cm^{-1} (Fig. 5c), which is the signature of Cu_2S as previously reported.[30,31]

The optical properties of the 13.5 nm Cu_2S nanocrystals were also studied by UV-vis-NIR absorption and photoluminescence (PL) emission spectroscopy. The Cu_2S nanocrystals exhibited a wide and continuous absorption over a wavelength range from 250 nm to 1400 nm, and a NIR emission centered at 960 nm under the 785 nm excitation (Fig. 5d). The Cu_2S nanocrystals showed a bandgap of 1.29 eV with a full width at half-maximum (FWHM) of 0.15 eV (Fig. S3†). Compared to bulk Cu_2S (1.2 eV),[22,23] the bandgap of Cu_2S nanocrystals was blue-shifted due to the quantum confinement effect.

These Cu_2S nanocrystals may be promising building blocks for use in photovoltaic devices as light absorber[32,33] and counter electrode materials.[34,35]

It is interesting to note that two-dimensional (2-D) assembly and three-dimensional (3-D) assembly of Cu_2S nanocrystals were observed on the samples deposited on the copper TEM grids after the evaporation of the solvent (*i.e.*, chloroform) (Fig. S4†). These self-assembled nanostructures reduced the exposed surface areas, and thus lowered the surface energy of Cu_2S nanocrystals. The formation of these intriguing 2D and 3D assemblies was a direct consequence of the interplay between the surface-capping ligand (*i.e.*, alkylthiol), the use of uniform Cu_2S nanocrystals, and the evaporation rate of chloroform as reported in previous studies,[26,29,36] substantiating that Cu_2S nanocrystals had regular shape and nearly monodisperse size distributions.

In addition to Cu_2S nanocrystals, semiconducting Cu_2O nanocrystals were also successfully crafted by the inert-gas-driven continuous microflow reactor. Cu_2O nanocrystals were synthesized[37] with some modifications adopted for the microflow reactor system. In a typical reaction, 0.5 g (2.15 mmol) of copper(II) nitrate hemi(pentahydrate) ($Cu(NO_3)_2{\cdot}2.5H_2O$, 98%, Alfa) and 1.43 g (12.9 mmol in terms of the repeating unit) of poly(vinyl pyrrolidone) (PVP, MW = 29 000, Sigma Aldrich) were dissolved in 100 mL of ethylene glycol (EG) to prepare the precursor solution. In this reaction system, EG served as the reducing agent and solvent, and PVP was the surface ligand. The oil bath was preheated to 150 °C. The precursor solution was then introduced into the microflow reactor system which was pretreated by flowing nitrogen for 1 h. The flow rate was controlled at 3 mL min^{-1} and 1.5 mL min^{-1}, which are equivalent to the reaction time of 10 min and 20 min, respectively. The Reynolds numbers Re calculated based on eqn (1) were approximately 2.8 and 1.4 at the flow rates of 3 mL min^{-1} and 1.5 mL min^{-1} respectively (Table 2), for the synthesis of Cu_2O nanocrystals, which were also far below the critical value (*i.e.*, 2100), suggesting laminar flows. The final Cu_2O nanocrystals were obtained after purification by centrifuging and rinsing with ethanol, and were readily soluble in ethanol as the surface of nanocrystals was capped by PVP as the ligand. The nanocrystal production rates (milligram per hour; mg h^{-1}) were approximately 276 mg h^{-1} and 138 mg h^{-1} at the flow rates of 3 mL min^{-1} and 1.5 mL min^{-1}, respectively.

Fig. 6 compares the TEM images of as-synthesized Cu_2O nanocrystals at different flow rates (*i.e.*, different reaction times) and the corresponding size distribution histograms are determined by statistical analysis. Clearly, the resulting Cu_2O nanocrystals were spherical in shape and had the average diameters of 241 ± 19 nm and 367 ± 30 nm for nanocrystals synthesized at the different reaction times, that is, 10 min and 20 min, respectively (Table 2). Such large-sized Cu_2O nanocrystals have been widely observed in the literature, which were largely due to their formation *via* instantaneous nucleation and growth by inter-particle aggregation.[37,38] The TEM image of a single Cu_2O nanocrystal revealed that it had a rough surface (Fig. 7a), and the corresponding SAED showed the ring-like patterns, suggesting the polycrystalline nature of Cu_2O nanocrystals (Fig. 7b). All the rings can be indexed to the diffraction from Cu_2O. The XRD peaks matched well with the standard spectrum of Cu_2O (JCPDS no. 65-3288; Fig. 7c). Furthermore, we also extended the present study to continuously synthesize plasmonic Ag nanocrystals using the inert-gas-driven microflow reactor (see the ESI† for the detailed procedures and results).

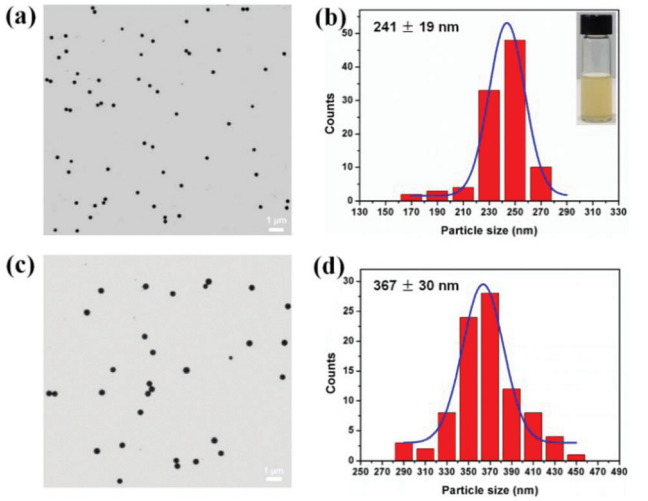

Fig. 6 TEM images and the corresponding size distribution histograms of Cu_2O nanocrystals synthesized at 150 °C at different flow rates: (a, b) 3 mL min^{-1} (corresponding to a reaction time of 10 min), (c, d) 1.5 mL min^{-1} (corresponding to a reaction time of 20 min). The blue curves are the Gaussian fittings of nanocrystal particle size distributions. The digital image of the 241 nm Cu_2O nanocrystals in ethanol is shown as an inset in (b).

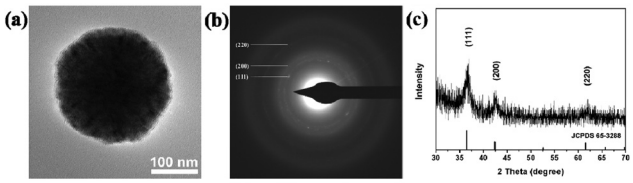

Fig. 7 (a) TEM image of a single Cu_2O nanocrystal, and (b) the corresponding SAED patterns. (c) XRD pattern of the 241 nm Cu_2O nanocrystals. The standard diffraction profile of Cu_2O (JCPDS no. 65-3288) is also shown at the bottom as a reference.

Table 2 Effect of the flow rate on the diameter of Cu_2S nanocrystals

Cu_2O sample	Flow rate (mL min^{-1})	Reaction time (min)	Reynolds number	Diameter (nm)
Fig. 6a	3	10	2.8	241 ± 19
Fig. 6c	1.5	20	1.4	367 ± 30

4. Conclusion

In summary, we demonstrated a facile and robust scalable strategy based on the implementation of a novel continuous microflow reactor driven by inert gas for the mass-production of uniform colloidal nanocrystals, especially easily-oxidized semiconducting nanocrystals. The size of nanocrystals was found to depend sensitively on the variations of the flow rate and the concentration of precursor solution. The inert-gas-driven microflow reactor strategy is general and enables good control over the nanocrystal size and scalability. It provides an attractive platform for crafting functional colloidal nanocrystals in large quantities with many applications in the areas of sensors, optics, electronics, solar energy conversion, photocatalysis and batteries.

We envision that by performing the continuous production of nanocrystals using rationally designed star-like block copolymers[39,40] (for plain and core/shell nanoparticles)[41] and bottlebrush-like block copolymers (for nanorods and nanotubes) as nanoreactors (*i.e.*, templates) inside a microflow reactor, a myriad of nanocrystals with high uniformity, diversified shapes, complex architectures, and superior long-term stability can be formed. This will be the subject of future studies.

Acknowledgements

We gratefully acknowledge financial support from the National Science Foundation (ECCS-1305087) (Z.L.) and the Academic Exchange Special Fund of University of Electronic Science and Technology of China (UESTC) for Overseas Training (H.T.).

Notes and references

1 T. K. Todorov, K. B. Reuter and D. B. Mitzi, *Adv. Mater.*, 2010, **22**, E156–E159.
2 J. Seo, M. J. Cho, D. Lee, A. Cartwright and P. N. Prasad, *Adv. Mater.*, 2011, **23**, 3984–3988.
3 M. G. Panthani, V. Akhavan, B. Goodfellow, J. P. Schmidtke, L. Dunn, A. Dodabalapur, P. F. Barbara and B. A. Korgel, *J. Am. Chem. Soc.*, 2008, **130**, 16770–16777.
4 Y. Liang, Y. Li, H. Wang, J. Zhou, J. Wang, T. Regier and H. Dai, *Nat. Mater.*, 2011, **10**, 780–786.
5 J. Chen, B. Lim, E. P. Lee and Y. Xia, *Nano Today*, 2009, **4**, 81–95.
6 X. Chen, S. Shen, L. Guo and S. S. Mao, *Chem. Rev.*, 2010, **110**, 6503–6570.
7 P. Z. Li, A. Aijaz and Q. Xu, *Angew. Chem., Int. Ed.*, 2012, **51**, 6753–6756.
8 J. S. Son, K. Park, M. K. Han, C. Kang, S. G. Park, J. H. Kim, W. Kim, S. J. Kim and T. Hyeon, *Angew. Chem., Int. Ed.*, 2011, **123**, 1399–1402.
9 H. Yang, L. A. Jauregui, G. Zhang, Y. P. Chen and Y. Wu, *Nano Lett.*, 2012, **12**, 540–545.
10 G. Hong, J. T. Robinson, Y. Zhang, S. Diao, A. L. Antaris, Q. Wang and H. Dai, *Angew. Chem., Int. Ed.*, 2012, **124**, 9956–9959.
11 P. Jiang, C.-N. Zhu, Z.-L. Zhang, Z.-Q. Tian and D.-W. Pang, *Biomaterials*, 2012, **33**, 5130–5135.
12 G. Lu, L. E. Ocola and J. Chen, *Adv. Mater.*, 2009, **21**, 2487–2491.
13 L. Zhang and Y. Xia, *Adv. Mater.*, 2014, **26**, 2600–2606.
14 L. Zhang, Y. Wang, L. Tong and Y. Xia, *Nano Lett.*, 2014, **14**, 4189–4194.
15 T. W. Phillips, I. G. Lignos and R. M. Maceiczyk, *Lab Chip*, 2014, **14**, 3172–3180.
16 H. Song, D. L. Chen and R. F. Ismagilov, *Angew. Chem., Int. Ed.*, 2006, **45**, 7336–7356.
17 A. Shavel, D. Cadavid, M. Ibanez, A. Carrete and A. Cabot, *J. Am. Chem. Soc.*, 2012, **134**, 1438–1441.
18 B. K. Yen, N. E. Stott, K. F. Jensen and M. G. Bawendi, *Adv. Mater.*, 2003, **15**, 1858–1862.
19 B. K. Yen, A. Günther, M. A. Schmidt, K. F. Jensen and M. G. Bawendi, *Angew. Chem., Int. Ed.*, 2005, **117**, 5583–5587.
20 E. M. Chan, R. A. Mathies and A. P. Alivisatos, *Nano Lett.*, 2003, **3**, 199–201.
21 X. Z. Lin, A. D. Terepka and H. Yang, *Nano Lett.*, 2004, **4**, 2227–2232.
22 H. Lee, S. W. Yoon, E. J. Kim and J. Park, *Nano Lett.*, 2007, **7**, 778–784.
23 Y. Wu, C. Wadia, W. Ma, B. Sadtler and A. P. Alivisatos, *Nano Lett.*, 2008, **8**, 2551–2555.
24 J. Chen, S. Deng, N. Xu, S. Wang, X. Wen, S. Yang, C. Yang, J. Wang and W. Ge, *Appl. Phys. Lett.*, 2002, **80**, 3620–3622.
25 L. Chen, Y. Xia, X. Liang, K. Yin, J. Yin, Z. Liu and Y. Chen, *Appl. Phys. Lett.*, 2007, **91**, 073511.
26 A. Tang, S. Qu, K. Li, Y. Hou, F. Teng, J. Cao, Y. Wang and Z. Wang, *Nanotechnology*, 2010, **21**, 285602.
27 H. Zhong, Y. Zhou, M. Ye, Y. He, J. Ye, C. He, C. Yang and Y. Li, *Chem. Mater.*, 2008, **20**, 6434–6443.
28 J. P. Holman, in *Heat Transfer*, McGraw-Hill, New York, 1986.
29 Z. Zhuang, Q. Peng, B. Zhang and Y. Li, *J. Am. Chem. Soc.*, 2008, **130**, 10482–10483.
30 S.-Y. Wang, W. Wang and Z.-H. Lu, *Mater. Sci. Eng., B*, 2003, **103**, 184–188.
31 C. Lai, Q. Wu, J. Chen, L. Wen and S. Ren, *Nanotechnology*, 2010, **21**, 215602.
32 S.-H. Wei, Q. Xu, B. Huang, Y. Zhao, Y. Yan and R. Noufi, Photovoltaic Specialists Conference (PVSC), 2012 38th IEEE, Austin, 2012.
33 Q. Xu, B. Huang, Y. Zhao, Y. Yan, R. Noufi and S.-H. Wei, *Appl. Phys. Lett.*, 2012, **100**, 061906.
34 J. G. Radich, R. Dwyer and P. V. Kamat, *J. Phys. Chem. Lett.*, 2011, **2**, 2453–2460.
35 Q. Shen, A. Yamada, S. Tamura and T. Toyoda, *Appl. Phys. Lett.*, 2010, **97**, 123107.

36 S. Li, H. Wang, W. Xu, H. Si, X. Tao, S. Lou, Z. Du and L. S. Li, *J. Colloid Interface Sci.*, 2009, **330**, 483–487.
37 M. H. Kim, B. Lim, E. P. Lee and Y. Xia, *J. Mater. Chem.*, 2008, **18**, 4069–4073.
38 J. Zhang, J. Liu, Q. Peng, X. Wang and Y. Li, *Chem. Mater.*, 2006, **18**, 867–871.
39 X. Pang, L. Zhao, M. Akinc, J. K. Kim and Z. Lin, *Macromolecules*, 2011, **44**, 3746–3752.
40 X. Pang, L. Zhao, C. Feng and Z. Lin, *Macromolecules*, 2011, **44**, 7176–7183.
41 X. Pang, L. Zhao, W. Han, X. Xin and Z. Lin, *Nat. Nanotechnol.*, 2013, **8**, 426–431.